

# Wavelets: application to turbulence

Marie Farge, LMD, Ecole Normale Supérieure, Paris, France,  
Kai Schneider, CMI, Université de Provence, Marseille, France

October 8, 2005

## Contents

<b>1</b>	<b>Introduction about turbulence and wavelets</b>	<b>3</b>
<b>2</b>	<b>Wavelet analysis</b>	<b>6</b>
2.1	Wavelet spectra . . . . .	6
2.2	Relation to classical analysis . . . . .	8
2.3	Intermittency measures . . . . .	9
<b>3</b>	<b>Wavelet compression</b>	<b>11</b>
3.1	Principle . . . . .	11
3.2	Extraction of coherent structures . . . . .	11
3.3	Application to three-dimensional turbulence . . . . .	13
<b>4</b>	<b>Wavelet computation</b>	<b>14</b>
4.1	Principle . . . . .	14
4.2	Adaptive wavelet scheme . . . . .	15
4.3	Application to two-dimensional turbulence . . . . .	16
<b>5</b>	<b>Further reading</b>	<b>17</b>

# 1 Introduction about turbulence and wavelets

## What is turbulence?

Turbulence is a highly nonlinear regime encountered in fluid flows. They are described by continuous fields, *e.g.*, velocity or pressure, assuming that the characteristic scale of the fluid motions is much larger than the mean free path of the molecular motions. The prediction of the space-time evolution of fluid flows from first principles is given by the solutions of the Navier-Stokes equations. The turbulent regime develops when the nonlinear term of Navier-Stokes equations strongly dominates the linear term; the ratio of the norms of both terms is the Reynolds number  $Re$ , which characterizes the level of turbulence. In this regime nonlinear instabilities dominate, which leads to the flow sensitivity to initial conditions and unpredictability. The corresponding turbulent fields are highly fluctuating and their detailed motions cannot be predicted, although, if one assumes some statistical stability of the turbulence regime, averaged quantities, such as mean and variance, or other related quantities, *e.g.*, diffusion coefficients, lift or drag, may still be predicted.

When turbulent flows are statistically stationary (in time) or homogeneous (in space), as it is classically supposed, one studies their energy spectrum, given by the modulus of the Fourier transform of the velocity auto-correlation. Unfortunately, since the Fourier representation spreads the information in physical space among the phase of all Fourier coefficients, the energy spectrum loses all structural information in time or space. This is a major limitation of the classical way of analyzing turbulent flows. This is why we have proposed to use the wavelet representation instead and define new analysis tools able to preserve time or space locality.

The same is true for computing turbulent flows. Indeed, the Fourier representation is well suited to studying linear phenomena, for which the superposition principle holds and whose generic behaviour is, either to persist at a given scale, or to spread to larger scales. In contrast, the superposition principle no more holds for nonlinear phenomena, their archetype being turbulent flows, which therefore cannot be decomposed as a sum of independent subsystems that can be separately studied. Generically their evolution involves a wide range of scales, exciting smaller and smaller ones, which could even lead to finite time singularities, *e.g.*, shocks. The 'art' of predicting the evolution of such nonlinear phenomena consists of disentangling the active from the passive elements: the former should be deterministically computed while the latter could, either be discarded or its effect could be statistically modelled. The wavelet representation allows to analyze the dynamics in both space and scale, retaining only those degrees of freedom which are essential to compute the flow evolution. Our goal is to perform a kind of 'distillation' in order to retain only the elements which are the essential to predict the nonlinear dynamics.

## How one studies turbulence?

When studying turbulence, one is uneasy about the fact that there are two different descriptions depending on which side of the Fourier transform one looks from.

- On the one hand, looking from the Fourier space representation, one has a theory that assumes the existence of a nonlinear cascade in an intermediate range of

spatial scales, called the 'inertial range', where energy is conserved and transferred towards small scales, but this on average only (considering either ensemble, or time or space averages). This implies that the flow is excited at large scales only and that dissipation acts at scales smaller than those of the inertial range. Under these hypotheses the theory predicts that the slope of the energy spectrum in the inertial range scales as  $k^{-5/3}$  in dimension three and as  $k^{-3}$  in dimension two,  $k$  being the modulus of the wave vector.

- On the other hand, if one studies turbulence from the physical space representation, there is not yet any universal theory. One relies instead on empirical observations, from both laboratory and numerical experiments, which exhibit the formation and persistence of coherent vortices, even at very high Reynolds numbers. Those coherent vortices correspond to the condensation of the vorticity field into some organized structures that contain most of the energy ( $L^2$ -norm of the velocity) and enstrophy ( $L^2$ -norm of the vorticity).

Moreover, the classical method for modelling turbulent flows consists in neglecting small scale motions and replacing them by their average, supposing the small scale dynamics to be either linear or slaved to the large scale motions. Such a method would work if there exists a clear separation between large and small scales, *i.e.* a spectral gap. Actually, there is now strong evidence, from both laboratory and direct numerical (DNS) experiments, that this is not the case. Conversely, one observes that turbulent flows are nonlinearly active all along the inertial range and that coherent vortices seem to play an essential dynamical role there, especially for transport and mixing. One may then ask the following questions: Are coherent vortices the elementary building blocks of turbulent flows? How can we extract them? Do their mutual interactions have an universal character? Can we compress turbulent flows and compute their evolution with a reduced number of degrees of freedom attached to the coherent vortices?

The direct numerical simulation (DNS) of turbulent flows, based on the integration of the Navier-Stokes equations using either grid points in physical space or Fourier modes in spectral space, requires a number of degrees of freedom per time step that varies as  $Re^{9/4}$  in dimension three (and as  $Re$  in dimension two). Due to the inherent limitation of computer performances, one can presently only perform DNS of turbulent flows up to Reynolds numbers  $Re = 10^6$ . To compute higher Reynolds flows, one should then design *ad hoc* turbulence models, for which some parameters are empirically adjusted to each type of flows, in particular to their geometry and boundary conditions, using data from either laboratory or numerical experiments.

### What are wavelets?

The wavelet transform unfolds signals (or fields) into both time (or space) and scale, and possibly directions in dimensions higher than one. The starting point is a function  $\psi \in L^2(\mathbb{R})$ , called the 'mother wavelet', which is well-localized in space  $x \in \mathbb{R}$  (it exhibits a fast decay for  $|x|$  tending to infinity), is oscillating ( $\psi$  has at least a vanishing integral, or better the first  $m$  moments of  $\psi$  vanish), and is smooth (its Fourier transform  $\hat{\psi}(k)$  exhibits fast decay for wavenumbers  $|k|$  tending to infinity). The mother wavelet then generates a family of wavelets,  $\psi_{a,b}(x) = a^{-1/2} \psi(\frac{x-b}{a})$ , by dilatation (or

contraction) by the scale parameter  $a \in \mathbb{R}^+$  and translation by the location parameter  $b \in \mathbb{R}$ , all wavelets being normalized in  $L^2$ -norm.

The wavelet transform of a function  $f \in L^2(\mathbb{R})$  is the inner product of  $f$  with the analyzing wavelets  $\psi_{a,b}$ , which gives the wavelet coefficients :  $\tilde{f}(a,b) = \langle f, \psi_{a,b} \rangle = \int f(x)\psi_{a,b}(x)dx$ . They measure the fluctuations of  $f$  around scale  $a$  and location  $b$ . The function  $f$  can be reconstructed without any loss as the inner product of its wavelet coefficients  $\tilde{f}$  with the analyzing wavelets  $\psi_{a,b}$  :  $f(x) = C_\psi^{-1} \int \int \tilde{f}(a,b)\psi_{a,b}(x)a^{-2}dadb$ ,  $C_\psi = \int |\hat{\psi}|^2|k|^{-1}dk$  being a constant which depends on the wavelet  $\psi$ .

Like the Fourier transform, the wavelet transform realizes a change of basis from physical space to wavelet space which is an isometry. It thus conserves the inner product (Plancherel theorem), and in particular energy (Parseval's identity). Let us mention that due to the localization of wavelets in physical space the behaviour of the signal at infinity does not play any role. Therefore, the wavelet analysis and synthesis can be performed locally, in contrast to the Fourier transform where the nonlocal nature of the trigonometric functions does not allow to perform a local analysis.

Moreover, wavelets constitute building blocks of various function spaces out of which some can be used to construct orthogonal bases. The main difference between the continuous and the orthogonal wavelet transforms is that the latter is non redundant, but preserves the invariance by translation and dilation only for a subset of wavelet space which corresponds to the dyadic grid  $\lambda = (j, i)$ , where scale is sampled by octaves  $j$  and space is sampled by locations  $2^{-j}i$ . The advantage is that all orthogonal wavelet coefficients are decorrelated, which is not the case for the continuous wavelet transform whose coefficients are redundant and correlated in space and scale. Such a correlation is easy to visualize by plotting the continuous wavelet coefficients of a white noise, and the patterns one thus observes are due to the reproducing kernel of the continuous wavelet transform, which corresponds to the correlation between the analyzing wavelets themselves.

In practice, to analyze turbulent signals or fields one should use the continuous wavelet transform with complex valued wavelets, since the modulus of the wavelet coefficients allows to read the evolution of the energy density in both space (or time) and scales. If one uses real-valued wavelets instead, the modulus of the wavelet coefficients will present the same oscillations as the analyzing wavelets and it will then become difficult to sort out features belonging to the signal or to the wavelet. In the case of complex-valued wavelets the quadrature between the real and the imaginary parts of the wavelet coefficients eliminates these spurious oscillations and this is why we recommend to use complex-valued wavelets, such as the Morlet wavelet. If one wants to compress turbulent flows, and *a fortiori* to compute their evolution at a reduced cost compared to standard methods (finite difference, finite volume or spectral methods), one should use orthogonal wavelets. In this case there is no redundancy, one has the same number of grid-points as wavelet coefficients, and there exists a fast wavelet transform algorithm which computes the orthogonal wavelet coefficients in  $O(N)$  operations, therefore faster than the fast Fourier transform whose operation count is  $O(N \log_2 N)$  only.

The first paper about the continuous wavelet transform has been published in 1984 (A. Grossmann and J. Morlet, 1984, *SIAM J. Appl. Anal.*, 15, 723). Then in 1986 discrete wavelets were constructed, leading to frames (I. Daubechies, A. Grossmann and Y. Meyer, 1986, *J. Math. Phys.*, 27, 1271) and orthogonal bases (P.-G. Lemarié and

*Y. Meyer, 1986, Revista Matematica Iberoamericana, 2, 1*). From there the formalism of multiresolution analysis (MRA) has been constructed which lead to the fast wavelet algorithm (*S. Mallat, 1989, Trans. Amer. Math. Soc., 315, 69*). The first application of wavelets to analyze turbulent flows has been published in 1988 (*M. Farge and G. Rabreau, C. R. Acad. Sci. Paris, 2, 307*). Since then a long-term research program has been developed for analyzing, computing and modelling turbulent flows using either continuous wavelets or orthogonal wavelets, and also wavelet packets.

## 2 Wavelet analysis

### 2.1 Wavelet spectra

#### Wavelet space

To study turbulent signals one uses the continuous wavelet transform for analysis, and the orthogonal wavelet transform for compression and computation. For the continuous wavelet transform, one can choose:

- either a real-valued wavelet, such as the Marr wavelet, also called 'Mexican hat', which is the second derivative of a Gaussian,

$$\psi(x) = (1 - x^2) \exp\left(\frac{-x^2}{2}\right) \quad , \quad (1)$$

- or a complex-valued wavelet, such as the Morlet wavelet,

$$\begin{aligned} \widehat{\psi}(k) &= \frac{1}{2\pi} \exp\left(-\frac{(k - k_\psi)^2}{2}\right) \quad \text{for } k > 0 \quad , \\ \widehat{\psi}(k) &= 0 \quad \text{for } k \leq 0 \quad . \end{aligned} \quad (2)$$

with the wavenumber  $k_\psi$  denoting the barycenter of the wavelet support in Fourier space

$$k_\psi = \frac{\int_0^\infty k |\widehat{\psi}(k)| dk}{\int_0^\infty |\widehat{\psi}(k)| dk} \quad . \quad (3)$$

For the orthogonal wavelet transform there is a large collection of possible wavelets and the choice depends on which properties are preferred, *e.g.*, compact-support, symmetry, smoothness, number of cancellations, computational efficiency.

From our own experience, we tend to prefer the Coifman wavelet 12, which is compactly supported, has four vanishing moments, is quasi-symmetric and is defined with a filter of length 12, which leads to a computational cost of the fast wavelet transform in  $24N$  operations since two filters are used.

As stated above, we recommend the complex-valued continuous wavelet transform for analysis. In this case, one then plots the modulus and the phase of the wavelet coefficients in wavelet space, with a linear horizontal axis corresponding to position  $b$ , and a logarithmic vertical axis corresponding to scale  $a$ , with the largest scale at the bottom and the smallest scale at the top.

In Fig. 5, we show the wavelet analysis of a turbulent signal (top), giving the time evolution of the velocity fluctuations of two successive vortex breakdowns, measured by hotwire anemometry at  $N = 32768 = 2^{15}$  instants (*Y. Kyupers and P. Petitjeans, PMMH, ESPCI, Paris*). The modulus of the wavelet coefficients (middle) shows that during the vortex breakdown, which is due to strong nonlinear flow instability, energy is spread over a wide range of scales. The phase of the wavelet coefficients (bottom) is plotted only where the modulus is non negligible, otherwise the phase information is meaning less. In Fig. 5 (bottom) one observes that the line of constant phase point towards the instants when the signal is less regular, *i.e.*, during vortex breakdowns.

### Local wavelet spectrum

Since the wavelet transform conserves energy and preserves locality in physical space, one can extend the concept of energy spectrum and define a local energy spectrum, such that

$$\tilde{E}(k, x) = \frac{1}{C_\psi k_\psi} \left| \tilde{f}\left(\frac{k_\psi}{k}, x\right) \right|^2 \quad \text{for } k \geq 0 \quad , \quad (4)$$

where  $k_\psi$  is the centroid wavenumber of the analyzing wavelet  $\psi$  and  $C_\psi$  is defined in the admissibility condition (respectively equations (10) and (1) in chapter 'Wavelets: theory').

By measuring  $\tilde{E}(k, x)$  at different instants or positions in the signal, one estimates what elements in the signal contribute most to the global Fourier energy spectrum, which might suggest a way to decompose the signal into different components. For example, if one considers turbulent flows, one can compare the energy spectrum of the coherent structures (such as isolated vortices in incompressible flows or shocks in compressible flows) and the energy spectrum of the incoherent background flow, since both elements exhibit different correlations and therefore spectral slopes.

### Global wavelet spectrum

Although the wavelet transform analyzes the flow using localized functions rather than complex exponentials, one can show that the global wavelet energy spectrum converges towards the Fourier energy spectrum provided the analyzing wavelet has enough vanishing moments. More precisely the global wavelet spectrum, defined by integrating (4) over all positions,

$$\tilde{E}(k) = \int_{-\infty}^{\infty} \tilde{E}(k, x) dx \quad (5)$$

gives the correct exponent for a power-law Fourier energy spectrum  $E(k) \propto k^{-\beta}$  if the analyzing wavelet has at least  $M > \frac{\beta-1}{2}$  vanishing moments. Thus, the steeper the energy spectrum one studies, the more vanishing moments the analyzing wavelet should have. The inertial range in turbulence has a power-law behaviour predicted by the statistical theory of homogeneous and isotropic turbulence. The ability to correctly evaluate the slope of the energy spectrum is an important property of the wavelet transform, related to its ability to detect and characterize singularities. We will not discuss here how wavelet coefficients could be used to study singularities and fractal measures, since it is presented in details in another chapter of this encyclopedia (*M. Yamada, Wavelets: Application, Effects and Implications*).

## 2.2 Relation to classical analysis

### Relation to Fourier spectrum

The global wavelet energy spectrum  $\tilde{E}(k)$  is actually a smoothed version of the Fourier energy spectrum  $E(k)$ . This can be seen from the following relation between the two spectra:

$$\tilde{E}(k) = \frac{1}{C_\psi k_\psi} \int_0^\infty E(k') \left| \hat{\psi} \left( \frac{k_\psi k'}{k} \right) \right|^2 dk' \quad , \quad (6)$$

which shows that the global wavelet spectrum is an average of the Fourier spectrum weighted by the square of the Fourier transform of the analyzing wavelets shifted at wavenumbers  $k$ . Note that the larger  $k$ , the larger the averaging interval, because wavelets are bandpass filters with  $\frac{\Delta k}{k}$  constant. This property of the global wavelet energy spectrum is particularly useful to study turbulent flows. Indeed, the Fourier energy spectrum of a single realization of a turbulent flow is too oscillating to be able to clearly detect a slope, while it is no more the case for the global wavelet energy spectrum, which is thus a better estimator of the spectral slope.

The real-valued Marr wavelet (1) has only two vanishing moments and thus can correctly measure energy spectrum exponents up to  $\beta < 5$ . In the case of the complex-valued Morlet wavelet (2), only the zeroth order moment is null, but the higher  $m^{\text{th}}$  order moments are very small ( $\propto k_\psi^m e^{-(k_\psi^2/2)}$ ), provided that  $k_\psi$  is larger than 5. For instance the Morlet wavelet transform with  $k_\psi = 6$  gives accurate estimates of the power-law exponent of the energy spectrum at least for  $\beta < 7$ .

There is also a family of wavelets with an infinite number of cancellations

$$\hat{\psi}_n(k) = \alpha_n \exp \left( -\frac{1}{2} \left( k^2 + \frac{1}{k^{2n}} \right) \right), \quad n \geq 1 \quad , \quad (7)$$

where  $\alpha_n$  is chosen for normalization. These wavelets can therefore correctly measure any power-law energy spectrum, and detect the difference between a power-law energy spectrum and a Gaussian energy spectrum ( $E(k) \propto e^{-(k/k_0)^2}$ ). For instance it is important in turbulence to determine the wavenumber after which the energy spectrum decays exponentially, since this wavenumber defines the end of the inertial range, dominated by nonlinear interactions, and the beginning of the dissipative range, dominated by linear dissipation.

### Relation to structure functions

In this section we will point out the limitations of classical measures of intermittency, and present a set of wavelet-based alternatives. The classical measures based on structure functions can be thought of as a special case of wavelet filtering using an extremely non-smooth wavelet defined as the difference of two Diracs (DOD). It is this lack of regularity of the underlying wavelet that limits the adequacy of classical measures to analyze sufficiently smooth signals. Wavelet-based diagnostics can overcome these limitations, and produce accurate results whatever the signal to be analysed.

We will link the scale dependent moments of the wavelet coefficients and the structure functions, which are classically used to study turbulence. In the case of second order statistics, the global wavelet spectrum corresponds to the second order structure



function. Furthermore, a rigorous bound for the maximum exponent of the structure functions is computed and there is a way to overcome this limitation by using wavelets.

The increments of a signal, also called the modulus of continuity, can be seen as its wavelet coefficients using the DOD wavelet

$$\psi^\delta(x) = \delta(x+1) - \delta(x) \quad . \quad (8)$$

We thus obtain

$$f(x+a) - f(x) = \tilde{f}_{x,a} = \langle f, \psi_{x,a}^\delta \rangle \quad , \quad (9)$$

with  $\psi_{x,a}(y) = 1/a[\delta((y-x)/a+1) - \delta((y-x)/a)]$ . Note that the wavelet is normalized with respect to the  $L^1$ -norm. The  $p$ -th order structure function  $S_p(a)$  therefore corresponds to the  $p$ -th order moment of the wavelet coefficients at scale  $a$ ,

$$S_p(a) = \int (\tilde{f}_{x,a})^p dx \quad . \quad (10)$$

As the DOD wavelet has only one vanishing moment (its mean), the exponent of the  $p$ -th order structure function in the case of a self-similar behaviour is limited by  $p$ , *i.e.*, if  $S_p(a) \propto a^{\zeta(p)}$  then  $\zeta(p) < p$ . To be able to detect larger exponents one has to use increments with a larger stencil, or wavelets with more vanishing moments.

We now concentrate on the case  $p = 2$ , *i.e.*, the energy norm. Equation (6) gives the relation between the global wavelet spectrum  $\tilde{E}(k)$  and the Fourier spectrum  $E(k)$  for an arbitrary wavelet  $\psi$ . For the DOD wavelet we find, since  $\widehat{\psi}^\delta(k) = e^{ik} - 1 = e^{ik/2}(e^{ik/2} - e^{-ik/2})$  and hence  $|\widehat{\psi}^\delta(k)|^2 = 2(1 - \cos k)$ , that

$$\tilde{E}(k) = \frac{1}{C_\psi k} \int_0^\infty E(k') \left( 2 - 2 \cos\left(\frac{k_\psi k'}{k}\right) \right) dk' \quad . \quad (11)$$

Setting  $a = k_\psi/k$  we see that the wavelet spectrum corresponds to the second order structure function, *i.e.*,

$$\tilde{E}(k) = \frac{1}{C_\psi k} S_2(a) \quad . \quad (12)$$

The above results show that, if the Fourier spectrum behaves like  $k^{-\alpha}$  for  $k \rightarrow \infty$ ,  $\tilde{E}(k) \propto k^{-\alpha}$  if  $\alpha < 2M + 1$ , where  $M$  denotes the number of vanishing moments of the wavelets. Consequently we find for  $S_2(a)$  that  $S_2(a) \propto a^{\zeta(2)} = \left(\frac{k_\psi}{k}\right)^{\zeta(2)}$  for  $a \rightarrow 0$  if  $\zeta(2) \leq 2M$ . In the present case we have  $M = 1$ , *i.e.*, the second order structure function can only detect slopes smaller than 2, corresponding to an energy spectrum with slopes shallower than  $-3$ . Thus we find that the usual structure function gives spurious results for sufficiently smooth signals. The relation between structure functions and wavelet coefficients can be generalized in the context of Besov spaces, which are classically used for nonlinear approximation theory (see chapter 'Wavelets: theory').

### 2.3 Intermittency measures

Intermittency is defined as localized bursts of high frequency activity. This means that intermittent phenomena are localized in both physical space and spectral space, and thus a suitable basis for representing intermittency should reflect this dual localization.

The Fourier basis is perfectly localized in spectral space, but completely delocalized in physical space. Therefore when a turbulence signal is filtered using a high-pass Fourier transform and then reconstructed in physical space, *e.g.*, to calculate the flatness, some spatial information is lost. This leads to smoothing of strong gradients and spurious oscillations in the background, which come from the fact that the modulus and phase of the discarded high wavenumber Fourier modes have been lost. The spatial errors introduced by such a Fourier filtering lead to errors in estimating the flatness, and hence the signal's intermittency.

When a quantity (*e.g.*, velocity derivative) is intermittent it contains rare but strong events (*i.e.*, bursts of intense activity), which correspond to large deviations reflected in the 'heavy tails' of the PDF. Second-order statistics (*e.g.*, energy spectrum, second-order structure function) are relatively insensitive to such rare events whose time or space supports are very small and thus do not dominate the integral. However, these events become increasingly important for higher-order statistics, and finally dominate. High-order statistics therefore characterize intermittency. Of course, intermittency is not essential for all problems: second-order statistics are sufficient to measure dispersion (dominated by energy-containing scales), but not to calculate drag or mixing (dominated by vorticity production in thin boundary or shear layers).

To measure intermittency one uses the space-scale information contained in the wavelet coefficients to define scale-dependent moments and moment ratios. Useful diagnostics to quantify the intermittency of a field  $f$  are the moments of its wavelet coefficients at different scales  $j$

$$M_{p,j}(f) = 2^{-j} \sum_{i=0}^{2^j-1} |\tilde{f}_{j,i}|^p \quad . \quad (13)$$

Note that the distribution of energy scale by scale, *i.e.*, the scalogram, can be computed from the second order moment of the orthogonal wavelet coefficients:  $E_j = 2^{j-1} M_{2,j}$ . Due to orthogonality of the decomposition the total energy is just the sum:  $E = \sum_{j \geq 0} E_j$ .

The sparsity of the wavelet coefficients at each scale is a measure of intermittency, and it can be quantified using ratios of moments at different scales

$$Q_{p,q,j}(f) = \frac{M_{p,j}(f)}{(M_{q,j}(f))^{\frac{p}{q}}} \quad , \quad (14)$$

which may be interpreted as quotient norms computed in two different functional spaces,  $L^p$ - and  $L^q$ -spaces. Classically, one chooses  $q = 2$  to define typical statistical quantities as a function of scale. Recall that for  $p = 4$  we obtain the scale dependent flatness  $F_j = Q_{4,2,j}$ . It is equal to 3 for a Gaussian white noise at all scales  $j$ , which proves that this signal is not intermittent in this case. The scale dependent skewness, hyperflatness and hyperskewness are obtained for  $p = 3, 5$  and 6, respectively. For intermittent signals  $Q_{p,q,j}$  increases with  $j$ .

## 3 Wavelet compression

### 3.1 Principle

To study complex signals we now propose to separate the rare and extreme events from the dense events, and then calculate their statistics independently for each one. A major difficulty in turbulence research is that there is no clear scale separation between these two kinds of events. This lack of ‘spectral gap’ in turbulence excludes Fourier filtering for disentangling these two behaviours. Since the rare events are well localized in physical space, one might try to use an on-off filter defined in physical space to extract them. However, this approach changes the spectral properties by introducing spurious discontinuities, adding an artificial scaling (*e.g.*,  $k^{-2}$  in one dimension) to the energy spectrum. To avoid these problems we use the wavelet representation, which combines both physical space and spectral space localizations (bounded from below by Heisenberg’s uncertainty principle). In turbulence the relevant rare events are the coherent vortices and the dense events correspond to the residual background flow. We have proposed a nonlinear wavelet filtering of the wavelet coefficients of vorticity to separate the coherent vortices from the residual background flow. We now detail the different steps of this procedure.

### 3.2 Extraction of coherent structures

#### Principle

We propose a new method to extract coherent structures from turbulent flows, as encountered in fluids (*e.g.*, vortices, shocklets) or plasmas (*e.g.*, bursts), in order to study their role in transport and mixing.

We first replace the Fourier representation by the wavelet representation, which keeps track of both time and scale, instead of frequency only. The second improvement consists in changing our viewpoint about coherent structures. Since there is not yet an universal definition of coherent structures in turbulent flows, we prefer starting from a minimal but more consensual statement about them, that everyone hopefully could agree with: ‘*coherent structures are not noise*’. Using this apophatic method we propose the following definition: ‘*coherent structures as what remains after denoising*’.

For the noise we use the mathematical definition stating that a noise cannot be compressed in any functional basis. Another way to say this is to observe that the shortest description of a noise is the noise itself. Notice that often one calls ‘noise’ what is actually ‘experimental noise’.

Considering our definition of coherent structures, turbulent signals can be split into two contributions: coherent bursts, corresponding to that part of the signal which can be compressed in a wavelet basis, plus incoherent noise, corresponding to that part of the signal which cannot be compressed, neither in wavelets nor in any other basis. We will then check *a posteriori* that the incoherent contribution is spread, and therefore does not compress, in both Fourier and grid point basis. Since we use the orthogonal wavelet representation, both coherent and incoherent components are orthogonal and therefore the  $L^2$ -norm, *e.g.*, energy or enstrophy, is a superposition of coherent and incoherent contributions.

Assuming that coherent structures are what remains after denoising, we need a model, not for the structures, but for the noise. As a first guess, we choose the simplest model and suppose the noise to be additive, Gaussian and white, *i.e.*, uncorrelated. Having this model in mind, we use Donoho's and Johnstones theorem to compute the value to threshold the wavelet coefficients. Since the threshold value depends on the variance of the noise, which in the case of turbulence is not *a priori* known, we propose a recursive method to estimate it from the variance of the weakest wavelet coefficients, *i.e.*, those whose modulus is below the threshold value.

### Wavelet decomposition

We describe the wavelet algorithm to extract coherent vortices out of turbulent flows and apply it as example the 3D turbulent flow. We consider the vorticity field  $\vec{\omega}(\vec{x}) = \nabla \times \vec{v}$ , computed at resolution  $N = 2^{3J}$ ,  $N$  being the number of grid points and  $J$  the number of octaves. Each component is developed into an orthogonal wavelet series from the largest scale  $l_{max} = 2^0$  to the smallest scale  $l_{min} = 2^{J-1}$  using a 3D multi-resolution analysis (MRA):

$$\begin{aligned} \omega(\vec{x}) &= \bar{\omega}_{0,0,0} \phi_{0,0,0}(\vec{x}) \\ &+ \sum_{j=0}^{J-1} \sum_{i_x=0}^{2^j-1} \sum_{i_y=0}^{2^j-1} \sum_{i_z=0}^{2^j-1} \sum_{d=1}^{2^n-1} \tilde{\omega}_{j,i_x,i_y,i_z}^d \psi_{j,i_x,i_y,i_z}^d(\vec{x}) \quad , \end{aligned} \quad (15)$$

with  $\phi_{j,i_x,i_y,i_z}(\vec{x}) = \phi_{j,i_x}(x) \phi_{j,i_y}(y) \phi_{j,i_z}(z)$ , and

$$\psi_{j,i_x,i_y,i_z}^d(\vec{x}) = \begin{cases} \psi_{j,i_x}(x) \phi_{j,i_y}(y) \phi_{j,i_z}(z) & ; d = 1 \quad , \\ \phi_{j,i_x}(x) \psi_{j,i_y}(y) \phi_{j,i_z}(z) & ; d = 2 \quad , \\ \phi_{j,i_x}(x) \phi_{j,i_y}(y) \psi_{j,i_z}(z) & ; d = 3 \quad , \\ \psi_{j,i_x}(x) \phi_{j,i_y}(y) \psi_{j,i_z}(z) & ; d = 4 \quad , \\ \psi_{j,i_x}(x) \psi_{j,i_y}(y) \phi_{j,i_z}(z) & ; d = 5 \quad , \\ \phi_{j,i_x}(x) \psi_{j,i_y}(y) \psi_{j,i_z}(z) & ; d = 6 \quad , \\ \psi_{j,i_x}(x) \psi_{j,i_y}(y) \psi_{j,i_z}(z) & ; d = 7 \quad , \end{cases} \quad (16)$$

where  $\phi_{j,i}$  and  $\psi_{j,i}$  are the one-dimensional scaling function and the corresponding wavelet, respectively. Due to orthogonality, the scaling coefficients are given by  $\bar{\omega}_{0,0,0} = \langle \omega, \phi_{0,0,0} \rangle$  and the wavelet coefficients are given by  $\tilde{\omega}_{j,i_x,i_y,i_z}^\mu = \langle \omega, \psi_{j,i_x,i_y,i_z}^\mu \rangle$ , where  $\langle \cdot, \cdot \rangle$  denotes the  $L^2$ -inner product.

### Nonlinear thresholding

The vorticity field is then split into  $\vec{\omega}_C(\vec{x})$  and  $\vec{\omega}_I(\vec{x})$  by applying a nonlinear thresholding to the wavelet coefficients. The threshold is defined as  $\epsilon = (4/nZ \ln N)^{1/2}$ , where  $n$  is the space dimension which is here  $n = 3$ . It only depends on the total enstrophy  $Z$  and on the number of grid points  $N$  without any adjustable parameters. The choice of this threshold is based on theorems by Donoho and Johnstone proving optimality of the wavelet representation to denoise signals in presence of Gaussian white noise, since this wavelet-based estimator minimizes the maximal  $L^2$ -error for functions with inhomogeneous regularity.

### Wavelet reconstruction

The coherent vorticity field  $\vec{\omega}_C$  is reconstructed from the wavelet coefficients whose modulus is larger than  $\epsilon$  and the incoherent vorticity field  $\vec{\omega}_I$  from the wavelet coefficients whose modulus is smaller or equal to  $\epsilon$ . The two fields thus obtained,  $\vec{\omega}_C$  and  $\vec{\omega}_I$ , are orthogonal, which ensures a separation of the total enstrophy into  $Z = Z_C + Z_I$  because the interaction term  $\langle \vec{\omega}_C, \vec{\omega}_I \rangle$  vanishes. We then use Biot–Savart’s relation  $\vec{v} = \nabla \times (\nabla^{-2} \vec{\omega})$  to reconstruct the coherent velocity  $\vec{v}_C$  and the incoherent velocity  $\vec{v}_I$  for the coherent and incoherent vorticities respectively.

### 3.3 Application to three-dimensional turbulence

We consider a three-dimensional homogeneous isotropic turbulent flow, computed by direct numerical simulation (DNS) on the ‘Earth Simulator’ in Yokohama (Japan) at resolution  $N = 2048^3$ , which corresponds to a Reynolds number based on the Taylor microscale  $R_\lambda = 732$  (Kaneda *et al.*, *Physics of Fluids*, **15**, 2003). The computation uses a pseudo-spectral code, with a Gaussian random vorticity field as initial condition, and the flow evolution is integrated until a statistically stationary state is reached. Fig. 5 shows the modulus of the vorticity fluctuations of the total flow, zooming on a  $64^3$  sub-cube to enhance structural details. The flow exhibits elongated, distorted and folded vortex tubes, as observed in laboratory and numerical experiments.

We apply to the total flow the wavelet compression algorithm described above. We find that only 2.6% wavelet modes correspond to the coherent flow, which retains 99% of the energy and 81% of the enstrophy, while the remaining 97.4% incoherent modes contain only 1% of the energy and 19% of the enstrophy. We display the modulus of the coherent (Fig. 5) and incoherent (Fig. 5) vorticity fluctuations resulting from the wavelet decomposition. Note that the values of the three iso-surfaces chosen for visualization ( $I\omega I = 3\sigma$ ,  $4\sigma$  and  $5\sigma$ , with  $\sigma = (2Z)^{\frac{1}{2}}$  the r.m.s. of the vorticity fluctuations) are the same for the total and coherent vorticities, but they have been reduced by a factor two for the incoherent vorticity whose fluctuations are much smaller. In the coherent vorticity (Fig. 5) we recognize the same vortex tubes as those present in the total vorticity (Fig. 5). In contrast, the remaining vorticity (Fig. 5) is much more homogeneous and does not exhibit coherent structures. Hence, the wavelet compression retains all the vortex tubes and preserves their structure at all scales. Consequently, the coherent flow is as intermittent as the total flow, while the incoherent flow is structureless and non-intermittent. Modelling the effect of the incoherent flow onto the coherent flow should then be simple.

Fig. 5 shows the velocity PDF in semilogarithmic coordinates. We observe that the coherent velocity has the same Gaussian distribution as the total velocity, while the incoherent velocity remains Gaussian, but its variance is much smaller.

The corresponding energy spectra are plotted on Fig. 5. We observe that the spectrum of the coherent energy is identical to the spectrum of the total energy all along the inertial range. This implies that vortex tubes are responsible for the  $k^{-\frac{5}{3}}$  energy scaling, which corresponds to a long-range correlation, characteristic of three dimensional turbulence as predicted by Kolmogorov’s theory. In contrast, the incoherent energy has a scaling close to  $k^2$ , which corresponds to an energy equipartition between all wavevectors  $\vec{k}$ , since the isotropic spectrum is obtained by integrating energy in 3D  $\vec{k}$ -space over two dimensional shells  $k = |\vec{k}|$ . The incoherent velocity field is therefore spatially decorre-

lated, which is consistent with the observation that incoherent vorticity is structureless and homogeneous (Fig. 5).

From these observations, we propose the following scenario to interpret the turbulent cascade: the coherent energy injected at large scales is transferred towards small scales by nonlinear interactions between vortex tubes. In the meantime these nonlinear interactions also produce incoherent energy at all scales, which is dissipated only at the smallest scales. Thus, the coherent flow causes direct transfer of the coherent energy into incoherent energy. Conversely, the incoherent flow does not trigger any energy transfer to the coherent flow, as it is structureless and decorrelated. We conjecture that the coherent flow is dynamically active, while the incoherent flow is slaved to it, being only passively advected and mixed by the coherent vortex tubes. This is a different view from the classical interpretation since it does not suppose any scale separation. Both coherent and incoherent flows are active all along the inertial range, but they are characterized by different probability functions and correlations, non-Gaussian and long-range correlated for the former, while Gaussian and correlated for the latter.

## 4 Wavelet computation

### 4.1 Principle

The mathematical properties of wavelets (see chapter '*Wavelets: theory*') motivate their use for solving of partial differential equations (PDEs). The localization of wavelets, both in scale and space, leads to effective sparse representations of functions and pseudo-differential operators (and their inverse) by performing nonlinear thresholding of the wavelet coefficients of the function and of the matrices representing the operators. Wavelet coefficients allow to estimate the local regularity of solutions of PDEs and thus can define auto-adaptive discretizations with local mesh refinements. The characterization of function spaces in terms of wavelet coefficients and the corresponding norm equivalences lead to diagonal preconditioning of operators in wavelet space. Moreover, the existence of the fast wavelet transform yields algorithms with optimal linear complexity.

The currently existing algorithms can be classified in different ways. We can distinguish between Galerkin, collocation and hybrid scheme. Hybrid schemes combine classical discretizations, *e.g.*, finite differences or finite volumes, and wavelets, which are only used to speed up the linear algebra and to define adaptive grids. On the other hand, Galerkin and collocation schemes employ wavelets directly for the discretization of the solution and the operators.

Wavelet methods have been developed to solve Burger's, Stokes, Kuramoto–Sivashinsky, nonlinear Schrödinger, Euler and Navier–Stokes equations. As example, we present an adaptive wavelet algorithm of Galerkin type to solve the two-dimensional Navier–Stokes equations.

## 4.2 Adaptive wavelet scheme

We consider the two-dimensional Navier–Stokes equations written in terms of vorticity  $\omega$  and stream-function  $\Psi$ , which are both scalars in two dimensions,

$$\partial_t \omega + \vec{v} \cdot \nabla \omega - \nu \nabla^2 \omega = \nabla \times \vec{F} \quad (17)$$

$$\nabla^2 \Psi = \omega \quad \text{and} \quad \vec{v} = \nabla^\perp \Psi \quad (18)$$

for  $\vec{x} \in [0, 1]^2$ ,  $t > 0$ . The velocity is denoted by  $\vec{v}$ ,  $\vec{F}$  is an external force,  $\nu > 0$  is the constant kinematic viscosity and  $\nabla^\perp = (-\partial_y, \partial_x)$ . The above equations are completed with boundary conditions and a suitable initial condition.

### Time discretization

Introducing a classical semi-implicit time discretization with a time step  $\Delta t$  and setting  $\omega^n(\vec{x}) \approx \omega(\vec{x}, n\Delta t)$  we obtain

$$(1 - \nu \Delta t \nabla^2) \omega^{n+1} = \omega^n + \Delta t (\nabla \times F^n - \vec{v}^n \cdot \nabla \omega^n) \quad (19)$$

$$\nabla^2 \Psi^{n+1} = \omega^{n+1} \quad \text{and} \quad \vec{v}^{n+1} = \nabla^\perp \Psi^{n+1} \quad (20)$$

Hence, in each time step two elliptic problems have to be solved and a differential operator has to be applied. Formally the above equations can be written in the abstract form  $Lu = f$ , where  $L$  is an elliptic operator with constant coefficients. This corresponds to a Helmholtz type equation for  $\omega$  with  $L = (1 - \nu \Delta t \nabla^2)$  and a Poisson equation for  $\Psi$  with  $L = \nabla^2$ .

### Spatial discretization

For the spatial discretization we use the method of weighted residuals, *i.e.*, a Petrov–Galerkin scheme. The trial functions are orthogonal wavelets  $\phi$  and the test functions are operator adapted wavelets, also called ‘vaguelettes’,  $\theta$ . To solve the elliptic equation  $Lu = f$  at time step  $t^{n+1}$  we develop  $u^{n+1}$  into an orthogonal wavelet series, *i.e.*,  $u^{n+1} = \sum_\lambda \tilde{u}_\lambda^{n+1} \psi_\lambda$ , where  $\lambda = (j, i_x, i_y, d)$  denotes the multi-index for scale  $j$ , space  $i$  and direction  $d$ . Requiring that the residual vanishes with respect to all test functions  $\theta_{\lambda'}$ , we obtain a linear system for the unknown wavelet coefficients  $\tilde{u}_\lambda^{n+1}$  of the solution  $u$ :

$$\sum_\lambda \tilde{u}_\lambda^{n+1} \langle L\psi_\lambda, \theta_{\lambda'} \rangle = \langle f, \theta_{\lambda'} \rangle \quad . \quad (21)$$

The test functions  $\theta$  are defined such that the stiffness matrix turns out to be the identity. Therefore the solution of  $Lu = f$  reduces to a change of the basis, *i.e.*  $u^{n+1} = \sum_\lambda \langle f, \theta_\lambda \rangle \psi_\lambda$ . The right-hand side  $f$  can then be developed into a biorthogonal operator adapted wavelet basis  $f = \sum_\lambda \langle f, \theta_\lambda \rangle \zeta_\lambda$ , with  $\theta_\lambda = L^{*-1} \psi_\lambda$  and  $\zeta_\lambda = L\psi_\lambda$ ,  $*$  denoting the adjoint operator. By construction  $\theta$  and  $\zeta$  are biorthogonal, *i.e.*, such that  $\langle \theta_\lambda, \mu_{\lambda'} \rangle = \delta_{\lambda, \lambda'}$ . It can be shown that both have similar localization properties in physical and Fourier space as  $\psi$ , and that they form a Riesz basis.

### Adaptive discretization

To get an adaptive space discretization for the problem  $Lu = f$  we consider only the significant wavelet coefficients of the solution. Hence, we only retain coefficients  $\tilde{u}_\lambda^n$

whose modulus is larger than a given threshold  $\varepsilon$ , *i.e.*,  $|\tilde{u}_\lambda^n| > \varepsilon$ . The corresponding coefficients are shown in Fig. 5 (white area under the solid line curve).

### Adaption strategy

To be able to integrate the equation in time we have to account for the evolution of the solution in wavelet coefficient space (indicated by the arrow in Fig. 5). Therefore we add at time step  $t^n$  the local neighbors to the retained coefficients, which constitute a security zone (grey domain in Fig. 5). The equation is then solved in this enlarged coefficient set (white and grey regions in Fig. 5) to obtain  $\tilde{u}_\lambda^{n+1}$ . Subsequently, we threshold the coefficients and retain only those with  $|\tilde{u}_\lambda^{n+1}| > \varepsilon$  (coefficients under the dashed curve in Fig. 5). This strategy is applied in each time step and hence allows to automatically track the evolution of the solution both in scale and space.

### Evaluation of the nonlinear term

For the evaluation of the nonlinear term  $f(u^n)$ , where the wavelet coefficients  $\tilde{u}^n$  are given, there are two possibilities:

- *Evaluation in wavelet coefficient space*

As illustration we consider a quadratic nonlinear term,  $f(u) = u^2$ . The wavelet coefficients of  $f$  can be calculated using the connection coefficients, *i.e.*, one has to calculate the bilinear expression,  $\sum_\lambda \sum_{\lambda'} \tilde{u}_\lambda \mathcal{I}_{\lambda\lambda'\lambda''} \tilde{u}_{\lambda'}$  with the interaction tensor  $\mathcal{I}_{\lambda\lambda'\lambda''} = \langle \psi_\lambda \psi_{\lambda'}, \theta_{\lambda''} \rangle$ . Although many coefficients of  $\mathcal{I}$  are zero or very small, the size of  $\mathcal{I}$  leads to a computation which is quite untractable in practice.

- *Evaluation in physical space*

This approach is similar to the pseudo-spectral evaluation of the nonlinear terms used in spectral methods, therefore it is called pseudo-wavelet technique. The advantage of this scheme is that general nonlinear terms, *e.g.*,  $f(u) = (1-u)e^{-C/u}$ , can be treated more easily. The method can be summarized as follows: starting from the significant wavelet coefficients,  $|\tilde{u}_\lambda| > \varepsilon$ , one reconstructs  $u$  on a locally refined grid and gets  $u(x_\lambda)$ . Then one can evaluate  $f(u(x_\lambda))$  pointwise and the wavelet coefficients  $\tilde{f}_\lambda$  are calculated using the adaptive decomposition.

Finally, one computes those scalar products of the r.h.s of (21) with the test functions  $\theta$  to advance the solution in time. We compute  $\tilde{u}_\lambda = \langle f, \theta_\lambda \rangle$  belonging to the enlarged coefficient set (white and grey regions in Fig. 5).

The algorithm is of  $O(N)$  complexity, where  $N$  denotes the number of wavelet coefficients used in the computation.

## 4.3 Application to two-dimensional turbulence

To illustrate the above algorithm we present an adaptive wavelet computation of a vortex-dipole impinging on a no-slip wall at Reynolds number  $R = 1000$  in a square container. To take into account the solid wall we use a volume penalisation method, for which both the fluid flow and the solid container are modelled as a porous medium whose porosity tends towards zero in the fluid and towards infinity in the solid region. The two-dimensional Navier-Stokes equations are thus modified by adding the forcing



term  $\vec{F} = -\frac{1}{\eta}\chi_{\Omega_s}\vec{V}$  in eq. 18, where  $\chi$  is the characteristic function whose value is one in the solid region and zero elsewhere. The equation are solved using the adaptive wavelet method in a periodic square domain of size 2.2, in which the square container of size 2 is imbedded, taking  $\eta = 10^{-3}$ . The maximal resolution corresponds to a fine grid of  $1024^2$  points.

Fig. 5 (left) shows snapshots of the vorticity field at times  $t = 0.2, 0.4, 0.6$  and  $0.8$  (in arbitrary units). We observe that the vortex-dipole is moving towards the wall and that strong vorticity gradients are produced when the dipole hits the wall. The computational grid is dynamically adapted during the flow evolution, since the nonlinear wavelet filter automatically refines the grid in regions where strong gradients develop. Fig. 5 (right) shows the centers of the retained wavelet coefficients at corresponding times. Note that during the computation only 5% out of  $1024^2$  wavelet coefficients are used. The time evolution of total kinetic energy and total enstrophy, squared norms of velocity and vorticity, respectively, are plotted in Fig. 5 to illustrate the production of enstrophy and the concomitant dissipation of energy when the vortex dipole hits the wall.

This computation illustrates the fact that the adaptive wavelet method allows an automatic grid refinement, both on the boundary layer at the wall but also in shear layers which develop during the flow evolution far from the wall. Therewith, the number of grid-points necessary for the computation is significantly reduced, and we conjecture that the resulting compression rate will increase with the Reynolds number.

## 5 Further reading

A. Cohen. Wavelet methods in numerical analysis. *Handbook of Numerical Analysis*. Eds. P.G. Ciarlet & J.L. Lions, Vol. 7, Elsevier, Amsterdam, 2000.

W. Dahmen. Wavelets and multiscale methods for operator equations. *Acta Numerica*, **6**, 55–228, Cambridge University Press, 1997.

I. Daubechies. *Ten lectures on wavelets*. SIAM, 1992.

M. Farge. Wavelet Transforms and their Applications to Turbulence. *Ann. Rev. Fluid Mech.*, Vol. 24, 395-457, 1992.

M. Farge, N. Kevlahan, V. Perrier & E. Goirand. Wavelets and Turbulence. *Proc. of the IEEE*, Vol. 84, n 4, 639-669, 1996.

M. Farge, N. Kevlahan, V. Perrier & K. Schneider. Turbulence analysis, modelling and computing using wavelets. *J.C. van den Berg (ed.), Wavelets in physics*, Cambridge University Press, pp. 117–200, 1999.

M. Farge & K. Schneider. Analysing and computing turbulent flows using wavelets. *New trends in turbulence. Les Houches 2000*, Vol. 74 (Eds. M. Lesieur, A. Yaglom & F. David), Springer, 449-503, 2002.

S. Mallat. *A wavelet tour of signal processing*. Academic Press, 1998.

K. Schneider, M. Farge & N. Kevlahan Spatial intermittency in two-dimensional turbulence *Woods Hole Mathematics, Perspectives in Mathematics and Physics*, eds. N. Tongring & R.C. Penner, 302–328, Word Scientific, 2004

Other papers about wavelets and turbulence can be download from:

[http : //wavelets.ens.fr](http://wavelets.ens.fr)

M.F. thankfully acknowledges Trinity College, Cambridge, U.K., and the Centre International de Rencontres Mathématiques (CIRM), Marseille, France, for hospitality while writing this paper. We are grateful the Association CEA–Euratom for financial support.

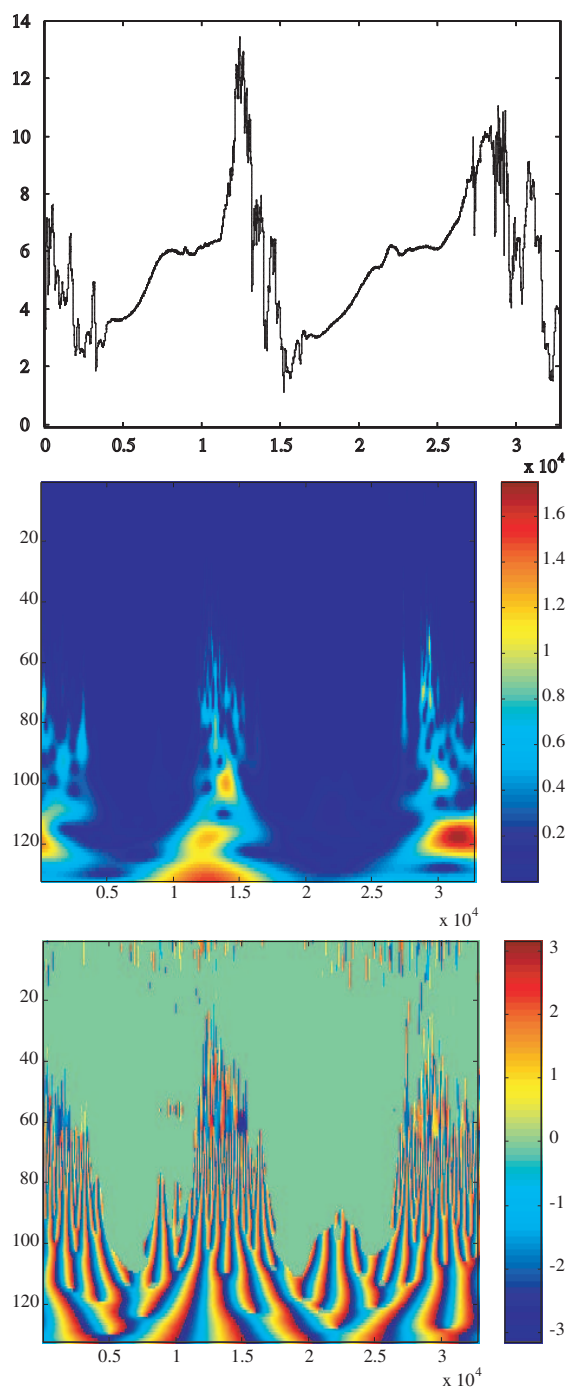


Figure 1: Example of a one-dimensional continuous wavelet analysis. Top: The signal to be analyzed. Middle: the modulus of its wavelet coefficients. Bottom: the phase of its wavelet coefficients.

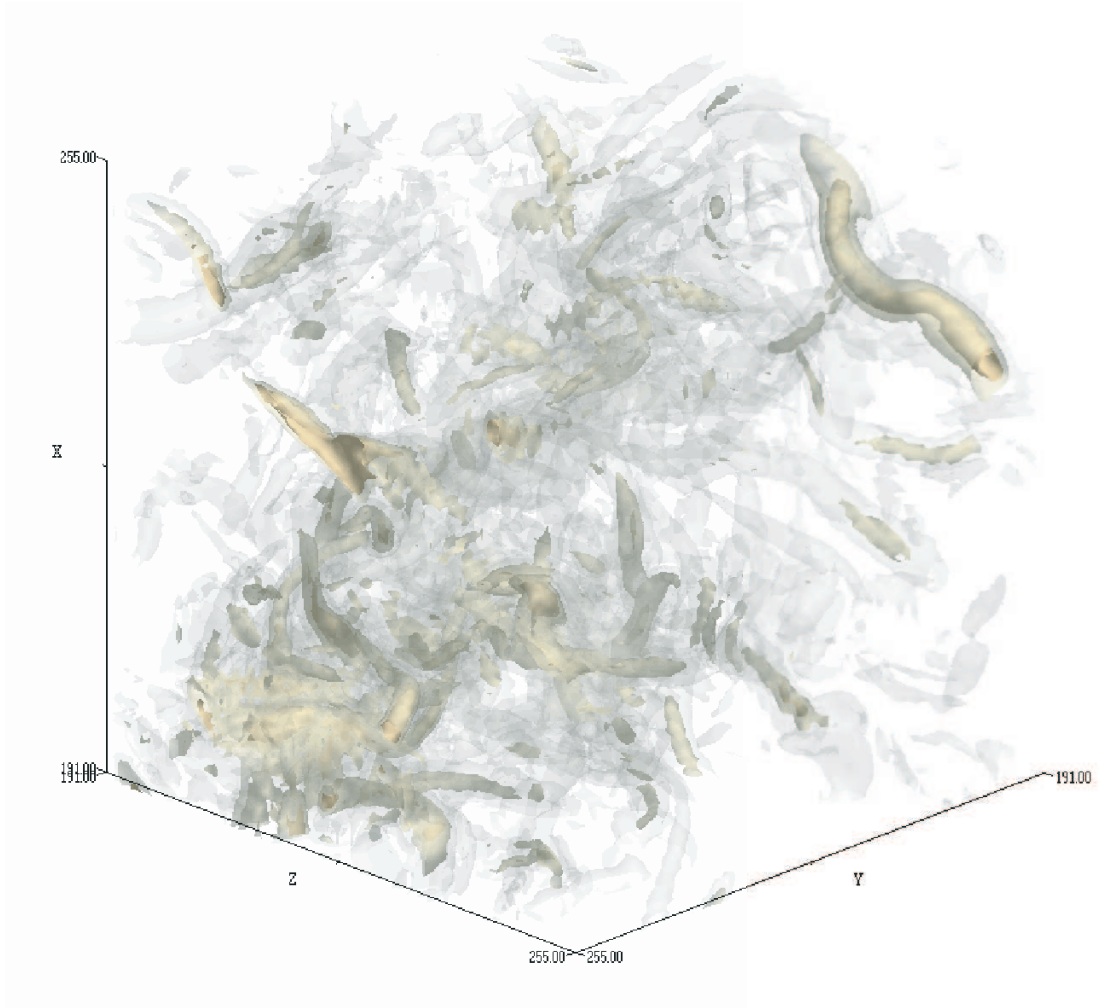


Figure 2: Isosurfaces of total vorticity, for  $|\vec{\omega}| = 150, 100, 50$  with opacity 1, 0.5, 0.1, respectively. Simulation with resolution  $N = 2048^3$  for  $R_\lambda = 732$ . Zoom on a sub-cube  $64^3$ .

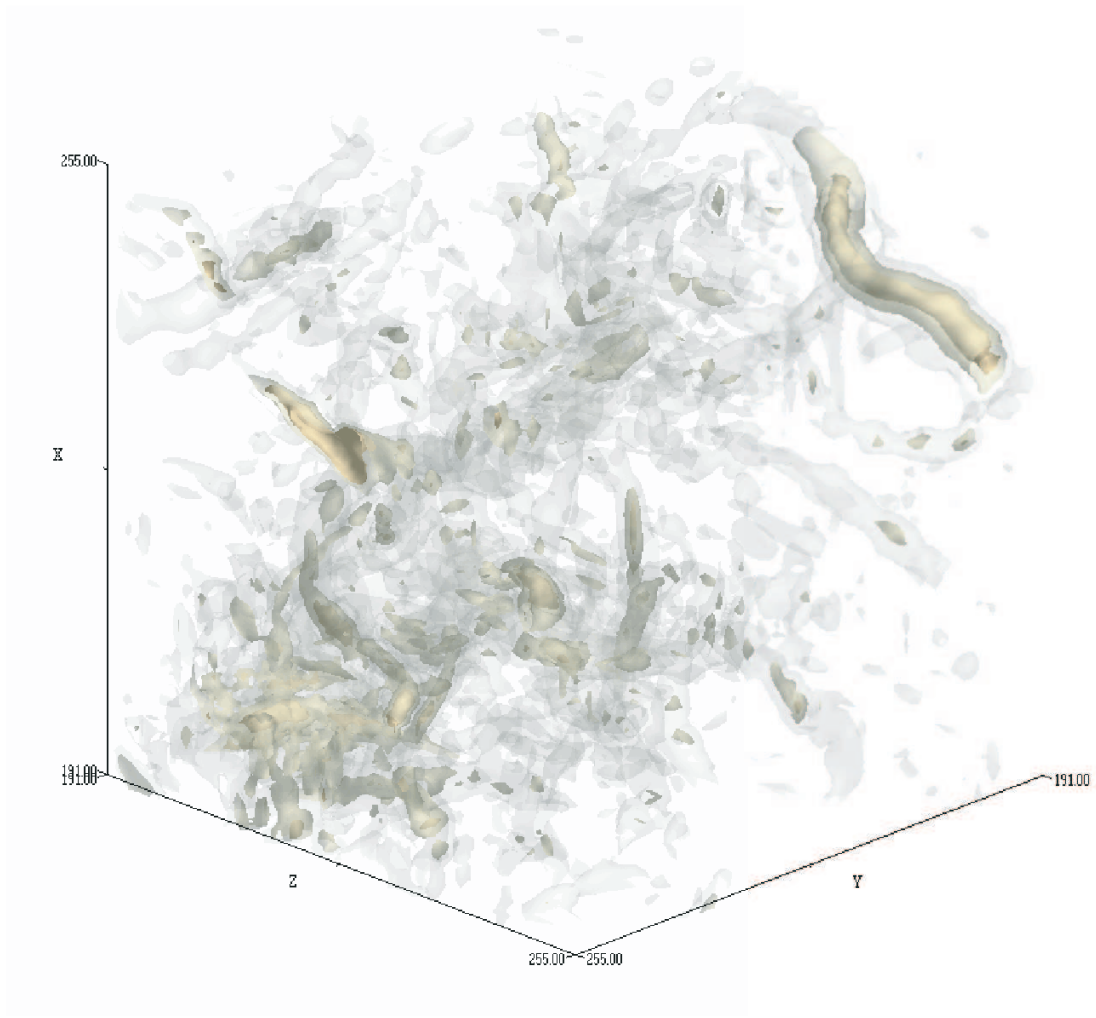


Figure 3: Isosurfaces of coherent vorticity, for  $|\vec{\omega}| = 150, 100, 50$  with opacity 1, 0.5, 0.1, respectively. Simulation with resolution  $N = 2048^3$ .

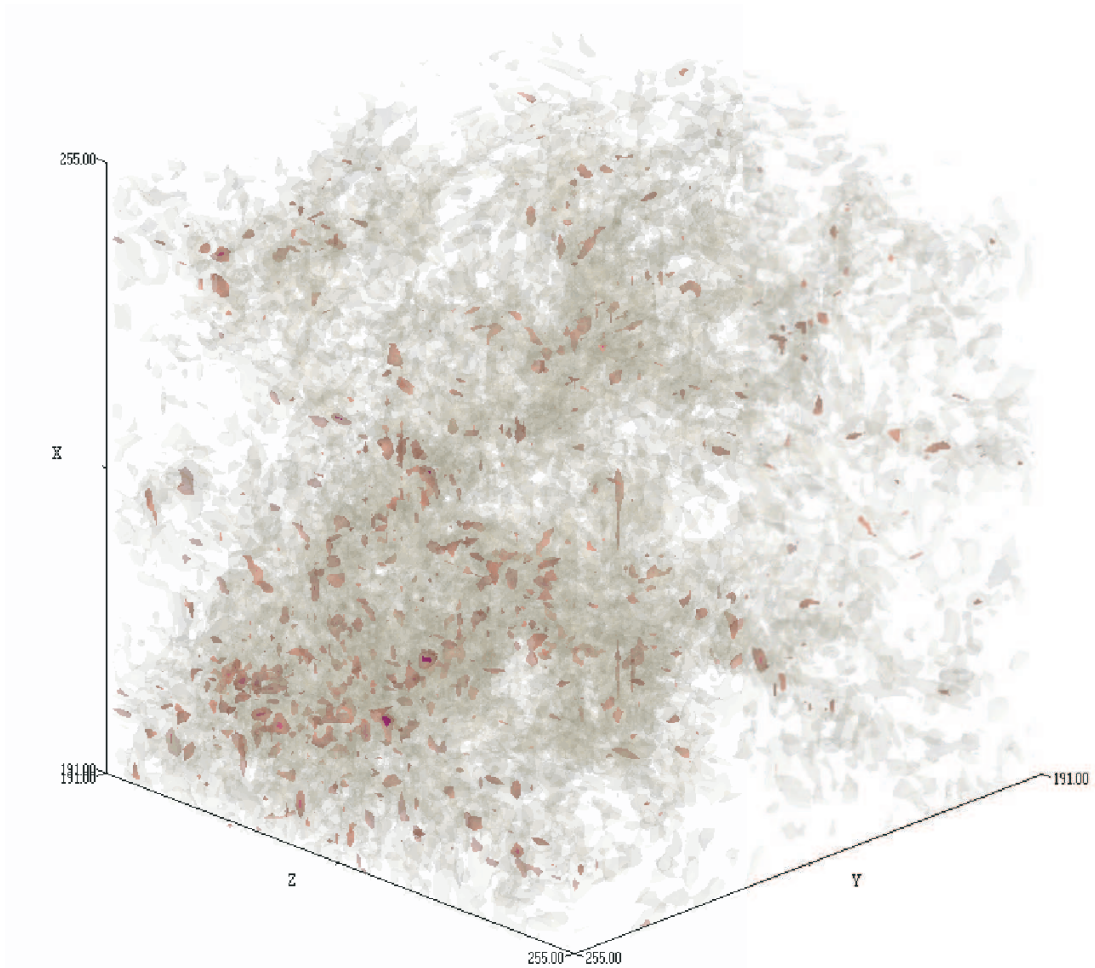


Figure 4: Isosurfaces of coherent vorticity, for  $|\vec{\omega}| = 75, 50, 25$  with opacity 1, 0.5, 0.1, respectively. Simulation with resolution  $N = 2048^3$ .

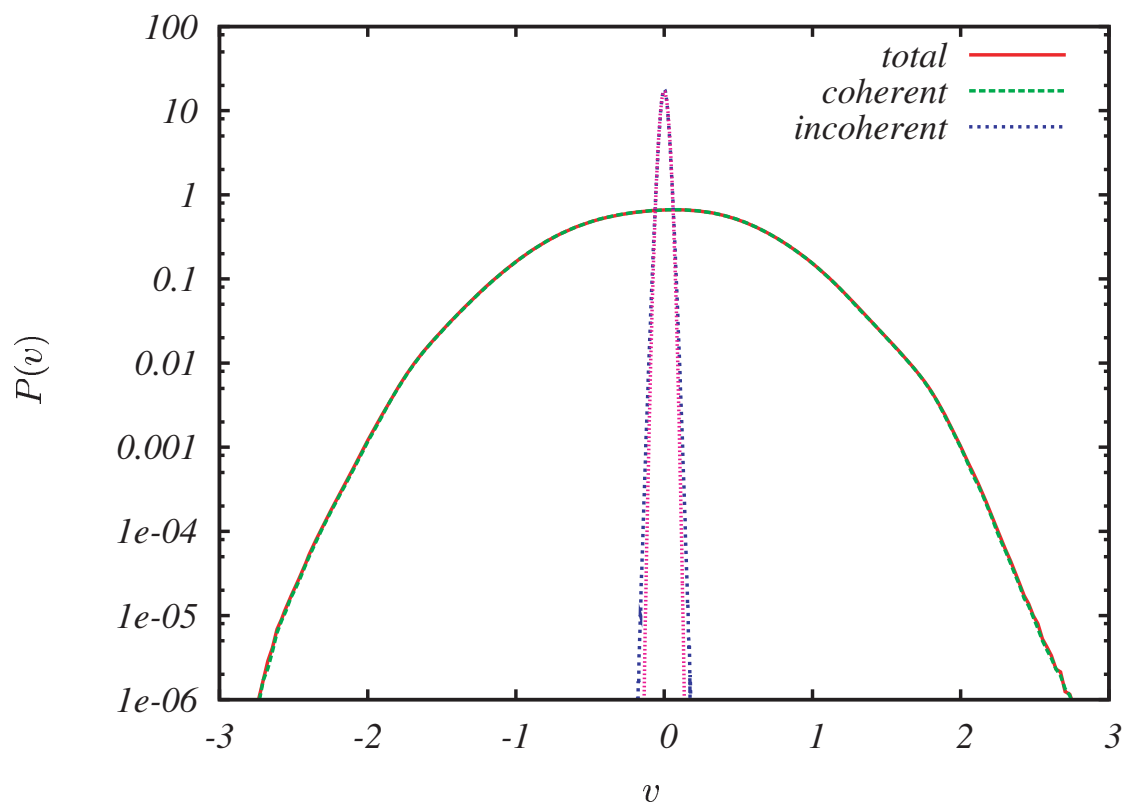


Figure 5: Velocity pdf, resolution  $N = 2048^3$  with a zoom at  $64^3$ .

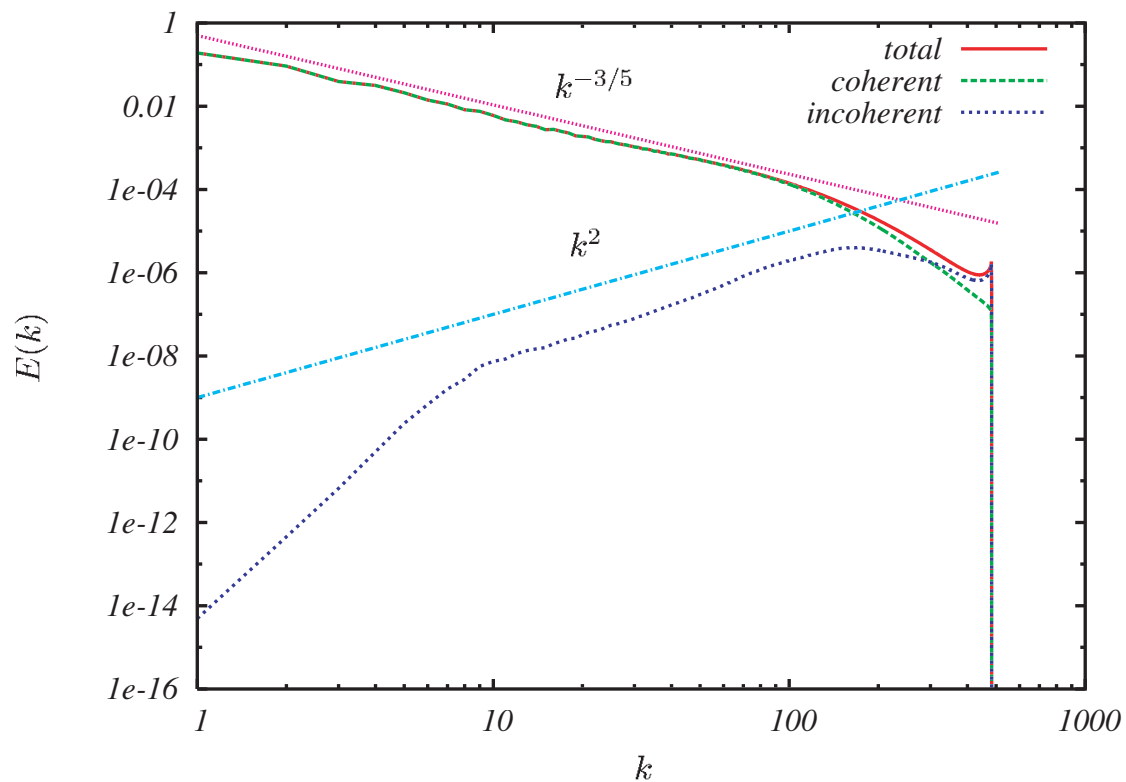


Figure 6: Energy spectrum, resolution  $N = 2048^3$  with a zoom at  $64^3$ .

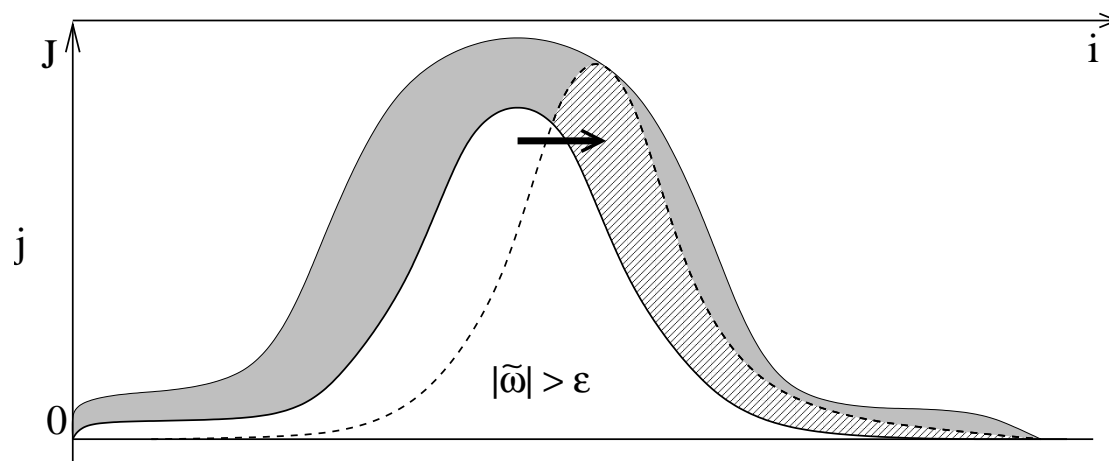


Figure 7: Illustration of the dynamic adaptation strategy in wavelet coefficient space.



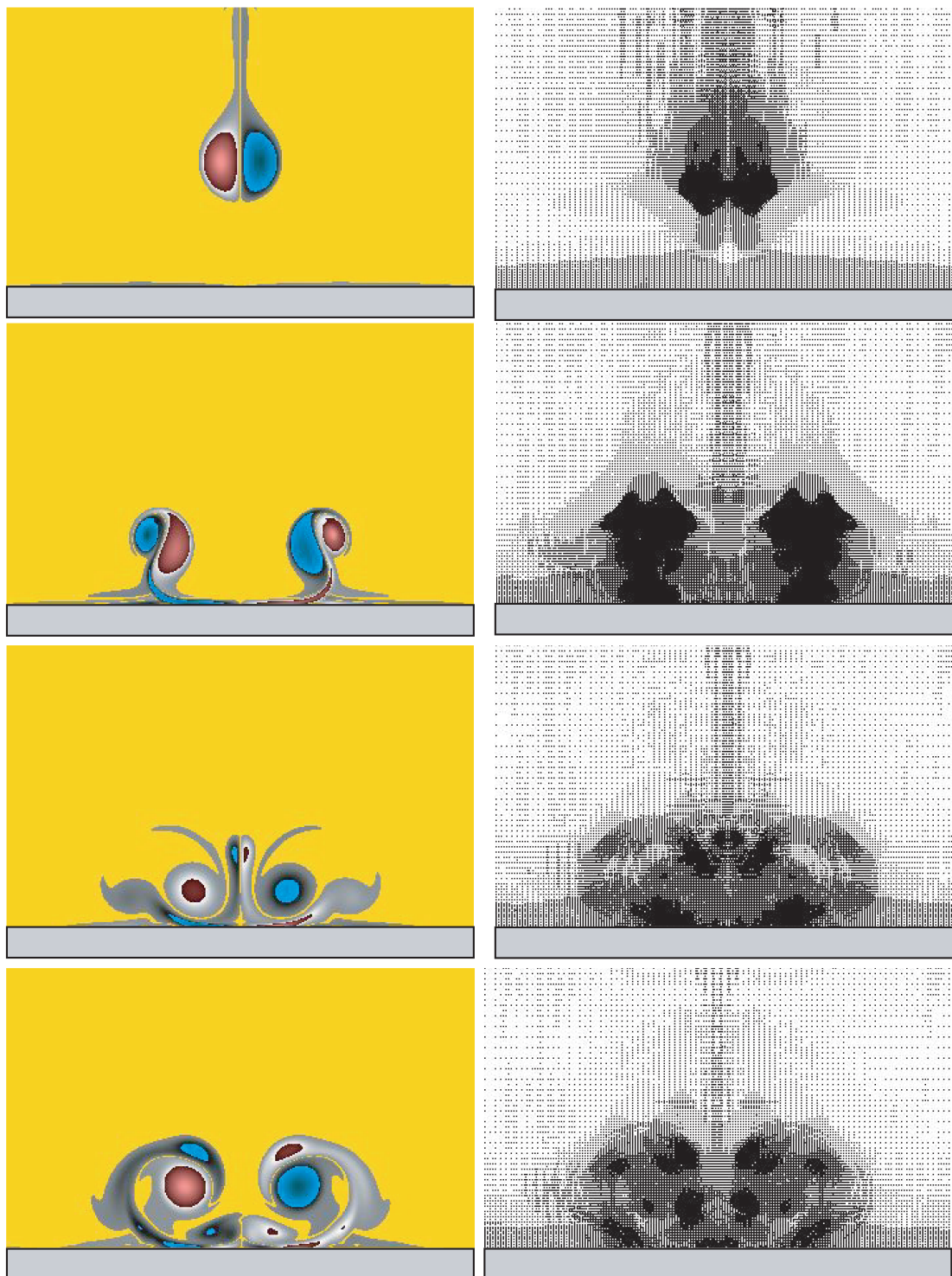


Figure 8: Dipole–wall interaction at  $Re = 1000$ . Vorticity fields (left), corresponding centers of active wavelets (right), at  $t = 0.2, 0.4, 0.6$  and  $0.8$  (from top to bottom).

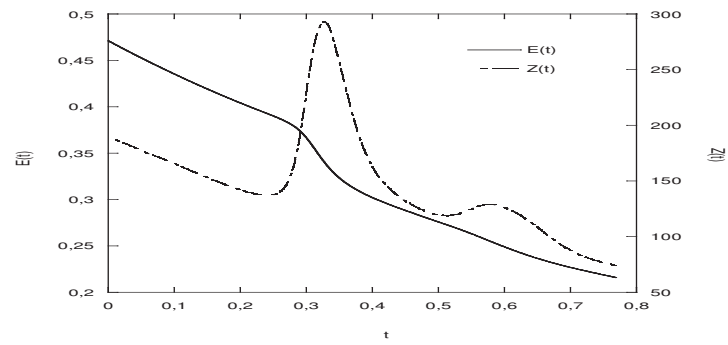


Figure 9: Time evolution of energy (solid line) and enstrophy (dotted line).